Final Scientific/Technical Report

Award Number:	DE-FG36-08GO88007
Recipient:	University of Nebraska at Kearney
Project Title:	CIBS Solar Cell Development
Covering Period:	July 1, 2008 to June 30, 2011
Date of Report:	September 28, 2011
Principal Investigator:	Christopher L. Exstrom Phone: 308-865-8565 Fax: 308-865-8399 Email: exstromc@unk.edu
Business Contact:	John Falconer, Director of Sponsored Programs Phone: 308-865-8565 Fax: 308-865-8399 Email: falconerj@unk.edu
Working Partners:	University of Nebraska-Lincoln
Cost-Sharing Partners:	University of Nebraska-Lincoln
DOE Project Team:	DOE Field Contracting Officer - Diana Bobo DOE Field Project Officer - Brian Hunter Financial Assistance Specialist - Christina Raines

Authorized Distribution Limitations: none

Executive Summary

Efforts to fabricate and study a new photovoltaic material, copper indium boron diselenide ($CuIn_xB_{1-x}Se_2$ or CIBS), were undertaken. Attempts to prepare CIBS using sputtering deposition techniques resulted in segregation of boron from the rest of elements in the material. CIBS nanocrystals were prepared from the reaction of elemental Se with CuCl, $InCl_3$, and boric acid in solution, but the product material quickly decomposed upon heating that was required in attempts to convert the nanocrystals into a thin film. The investigation of the reasons for the lack of CIBS material stability led to new structure-property studies of closely-related photovoltaic systems as well as studies of new solar cell materials and processing methods that could enhance the development of next-generation solar technologies. A detailed compositional study of $CuIn_{1-x}Al_xSe_2$ (CIAS, a system closely related to CIBS) revealed a non-linear correlation between crystal lattice size and the Al/(In+Al) ratios with dual-phase formation being observed. A new nanocrystal-to-thin-film processing method was developed for the preparation of $CuIn_{1-x}Ga_xSe_2$ (CIGS) thin films in which colloidal Se particles are sprayed in contact with $CuIn_{1-x}Ga_xS_2$ nanoparticles and heated in an argon atmosphere with no other Se source in the system. The process is non-vacuum and does not require toxic gases such as Se vapor or H_2Se. Expertise gained from these studies was applied to new research in the preparation of thin-film pyrite FeS_2, an attractive earth-abundant candidate material for next-generation photovoltaics. Three methods successfully produced pure pyrite FeS_2 films: sulfurization of sputtered Fe films, chemical bath deposition, and sulfurization of Fe_2O_3 sol-gel precursors. The last method produced pinhole-free films that may be viable for device development. Nickel, platinum, and possibly carbon would appear to serve as good ohmic contact materials. While CdS has a reasonable conduction band energy match to serve as an n-type buffer material in a pyrite FeS_2-based solar cell, the less toxic SnS_2 is being explored for this purpose.

Comparison of Actual Accomplishments with Project Goals and Objectives

Task 1.0 – Solvothermal Preparation and Characterization of Nanocrystalline $CuIn_{1-x}B_xSe_2$ (CIBS) Materials

- *Subtask 1.1 – Optimization of CIBS Preparation Reaction Conditions (Project milestone: Determination of reaction conditions that produce a single-phase CIBS nanocrystalline material)*

This subtask was completed. Refluxing CuCl, $InCl_3$, H_3BO_3, and Se in oleylamine under an argon atmosphere for 30 minutes yielded a black, nanocrystalline material that was characterized by micro-Raman spectroscopy as having a significantly higher A_1 phonon frequency (182 cm^{-1}) than that for CIS (170-172 cm^{-1}). This was indicative of boron incorporation into the chalcopyrite structure and the formation of a CIBS material. X-ray diffraction patterns matched those of CIS, suggesting that boron incorporation did not alter unit cell parameters, possibly due to boron occupying interstitial sites in the crystalline lattice.

- *Subtask 1.2 -- Determination of Boron Composition Control (Project milestone: Preparation of single-phase CIBS nanocrystalline materials of at least three different In/B ratios)*

This subtask was not completed. Due to the instability of nanocrystalline CIBS toward annealing temperatures required to form thin films (see Subtask 1.3 comments), CIBS samples with different In/B ratios could not be prepared. New studies on sythnesis of nanocrystalline $CuIn_{1-x}Al_xSe_2$ and selenization of $CuIn_{1-x}Al_x$ alloy films were undertaken to better understand Group 13 metal composition control in this similar quaternary chalcopyrite material that could be used as a model for understanding CIBS. Our group prepared the world's first $CuIn_{1-x}Al_xSe_2$ (x = 0.25, 0.5) nanocrystals. However, the non-uniform Al distributions observed led to a more thorough study of selenization of $CuIn_{1-x}Al_x$ over a broader Group 13 metal composition range (x = 0, 0.06, 0.18, 0.39, 0.64, 0.80, 1) that revealed a non-linear correlation between lattice constants and the composition parameter x. Additionally, dual-phase ($CuIn_{1-x}Al_xSe_2$/CuSe) formation was observed at mid-range Al/(In+Al) ratios.

- *Subtask 1.3 -- Conversion of Nanocrystalline CIBS to Thin-film form (Project milestone: Successful conversion of authenticated nanocrystalline CIBS sample (subtask 1.1) into thin-film form)*

This subtask was not completed due to the instability of the CIBS material prepared in Subtask 1.1 toward attempted annealing conditions (200-750 ^oC, 20 minutes to 4 hours, vacuum, N_2, Ar atmospheres) required to convert the as-made CIBS nanocrystals to a thin film. Sample Raman frequencies shifted from 182 to 173 cm^{-1} over a two-hour period, suggesting that boron phase-separated from CIS and evaporated as B_2Se_3 or other volatile species.

One other nanocrystal-to-thin-film processing method that was explored was the preparation of a quaternary chalcopyrite sulfide precursor followed by the reaction with selenium to form the quaternary chalcopyrite selenide. We were unable to prepare stable, pure $CuIn_{1-x}B_xS_2$ nanoparticles to serve as CIBS precursors; however, this route was studied for the preparation of $CuIn_{1-x}Ga_xSe_2$ (CIGS, x = 0, 0.25, 0.5, 0.75, 1) with the novel aspect that the only source of Se in the second reaction was a layer of colloidal Se particles sprayed on the $CuIn_{1-x}Ga_xS_2$ nanoparticle precursor. Upon heating at 550 ^oC for 60 minutes in an Ar atmosphere, Se displaced the sulfur in the$CuIn_{1-x}Ga_xS_2$ to form CIGS at all compositions. Reversing the layering order enables CIGS film preparation on Mo-coated glass substrates.

Task 2.0 -- Preparation of Thin-Film CIBS using *in-situ* Selenization *(Project milestone: Preparation of single-phase, thin-film CIBS material using one of the above methods)*

This task was not completed. $Cu_{.45}In_{.55-x}B_x$ precursor films of varying boron concentration (22-63%) were deposited on molybdenum coated stainless steel in order to facilitate higher selenization/sulfurization temperatures. Selenization/sulfurization temperatures of 550, 650, and 750 ^oC were used. In all cases, the resultant films peeled off the substrate or did not form the desired chalcopyrite with incorporated boron. Experiments repeated on quartz substrates in order to attain higher temperatures also failed to yield CIBS films.

Expertise gained from these and previous *ex-situ* selenization studies was applied to new studies in the preparation of thin-film pyrite FeS_2, an attractive earth-abundant candidate material for next-generation photovoltaics. Three methods successfully produced pure pyrite FeS_2 films: sulfurization of sputtered Fe films, chemical bath deposition, and sulfurization of Fe_2O_3 sol-gel precursors. The last method produced pinhole-free films that may be viable for device development. Nickel, platinum, and possibly carbon would appear to serve as good ohmic contact materials. While CdS has a reasonable conduction band energy match to serve as an n-type buffer material in a pyrite FeS_2-based solar cell, the less toxic SnS_2 is being explored for this purpose.

Task 3.0 -- Preparation of Thin-Film CIBS using *in-situ* Selenization *(Project milestones: 1) Demonstration of CIBS photovoltaic activity; 2) Determination of relationship between CIBS photovoltaic activity and boron concentration (based on at least three different CIBS films))*

As neither the Subtask 1.3 or Task 2.0 milestones were reached, this task could not be completed.

Task 4.0 Project Management and Reporting

Throughout the life the grant, the PI (Exstrom) coordinated and managed the project. Quarterly reports were provided to DOE in compliance with award policies.

Project Activity Summary

Project Objective: The fabrication and study of a new photovoltaic material, copper indium boron diselenide, $CuIn_xB_{1-x}Se_2$ (CIBS) will be undertaken in order to explore the feasibility of exceeding known energy conversion efficiencies of $CuIn_{1-x}Ga_xSe_2$ (CIGS) through alternative chemical composition changes.

Background: This project iss consistent with the DOE EERE Solar Energy Technologies Program, CIGS PV roadmap metric (2)(c), Develop, characterize, and understand alternative device structures and new materials so as to increase bandgap and VOC and minimize use of In. The most efficient thin-film solar cell to date (19.5%), is one with a $CuIn_{.70}Ga_{.30}Se_2$ (CIGS) absorber layer and a bandgap of 1.15 eV. As a consequence of bandgap structure changes that occur upon increasing gallium concentration, research has begun on substituting In with different group 13 elements in attempts to increase the bandgap to the theoretical optimum near 1.37 eV. We aim to fabricate and study a new material, copper indium boron diselenide, $CuIn_xB_{1-x}Se_2$ (CIBS). Boron is the lightest element in group 13 and should yield a higher bandgap for lower concentrations of boron than either gallium or aluminum. This lower concentration should lead to thin ordered films approaching those of $CuInSe_2$ (CIS) crystalline lattice parameters.

Status:

Task 1.0 [Solvothermal Preparation and Characterization of Nanocrystalline $CuIn_{1-x}B_xSe_2$ (CIBS) Materials].

Refluxing CuCl, $InCl_3$, H_3BO_3, and Se in oleylamine under an argon atmosphere for 30 minutes yielded a black, nanocrystalline material that was characterized by micro-Raman spectroscopy as having a significantly higher A_1 phonon frequency (182 cm^{-1}) than that for CIS (170-172 cm^{-1}). This was indicative of boron incorporation into the chalcopyrite structure and the formation of a CIBS material. X-ray diffraction patterns matched those of CIS, suggesting that boron incorporation did not alter unit cell parameters, possibly due to boron occupying interstitial sites in the crystalline lattice.

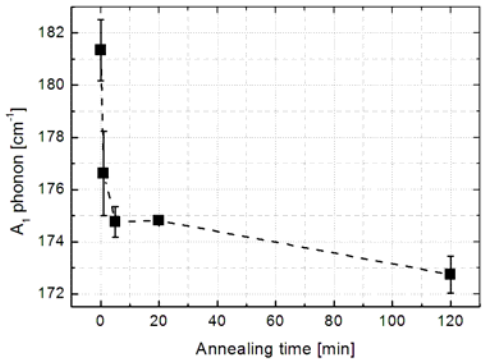

Figure 1. A_1 Phonon Frequencies of Nanocrystalline CIBS after Various Annealing Times (500 ^oC)

Annealing this CIBS material under vacuum, Ar, or N_2 at 500 ^oC resulted in a Raman frequency shift from 182 to 173 cm^{-1} over a two-hour period (Figure 1). This suggested that boron phase-separated from CIS.

In an effort to gain understanding of boron phase-separation, we conducted studies of annealing effects on material structures of model chalcopyrites. Toward this end, we reported the preparation, characterization, and studies of the world's first authenticated $CuIn_{1-x}Al_xSe_2$ (CIAS) nanocrystalline material [1].

Refluxing CuCl, $InCl_3$, Al(oleate)$_3$, and Se in oleylamine under an argon atmosphere for 30 minutes resulted in a black, nanocrystalline material that was characterized by scanning electron microscopy (SEM), X-ray diffraction (XRD), and micro-Raman spectroscopy. SEM images (Figure 2) revealed a mixture of hexagonal plate (500-2000 nm diameter), isomorphic, and irregular crystal morphologies that were likely due to non-uniform Al distributions through the material sample. Small nano-nodules (10-50 nm diameter) were observed through the material. XRD patterns (Figure 3) were consistent with a chalcopyrite structure and the increase in diffraction angles relative to those for CIS is indicative of aluminum incorporation. Raman spectroscopy shows an A_1 phonon frequency (180 cm^{-1}) that is shifted relative to that for CIS (170-172 cm^{-1}). This further supports aluminum incorporation. The optical bandgap for this sample was measured to be 1.26 eV.

Annealing this CIAS material under vacuum, Ar, or N_2 at 500 ^oC resulted in a Raman frequency shift from 180 to 177 cm^{-1} over a two-hour period (Figure 4). This suggested that aluminum phase-separates from CIS, but not to the degree that boron does when CIBS is annealed.

Use of Raman spectroscopy was deemed critical for further elucidation of the non-uniform distributions of aluminum that could occupy both interstitial and substitutional sites in the chalcopyrite crystal lattice in the nanocrystalline CIAS samples. However, as there had been no scientific studies correlating these spectroscopic properties to aluminum content in CIAS, we established correlations of A_1 phonon frequencies

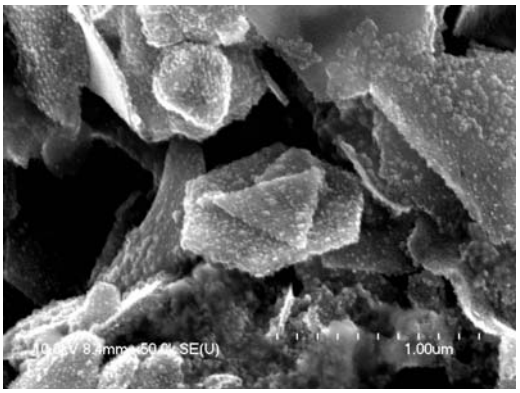

Figure 2. SEM image of CIAS nanocrystalline material before annealing. Scale: image width = 2.5 μm

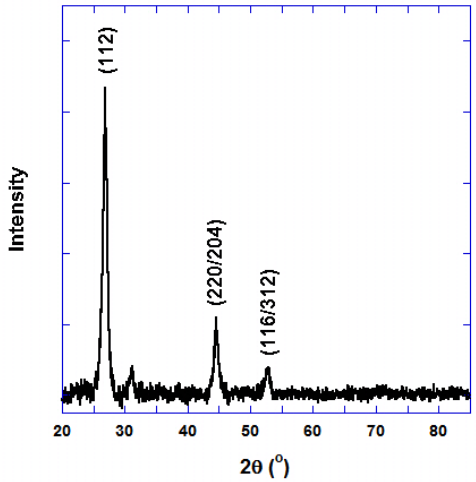

Figure 3. XRD pattern for CIAS nanocrystalline material before annealing.

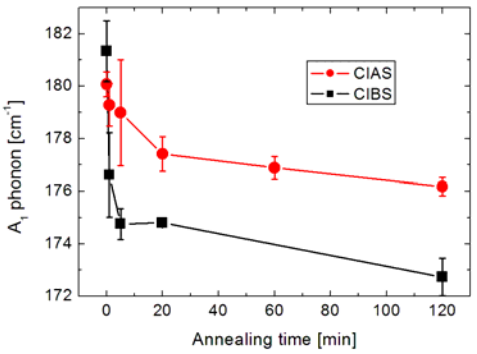

Figure 4. A_1 phonon frequencies of nanocrystalline CIBS and CIAS as a function of annealing time (500 ^oC)

and lattice parameters to Al/(In+Al) ratio in thin-film CIAS [2].

$CuIn_{1-x}Al_xSe_2$ thin films were deposited onto soda lime glass (SLG) by a two-step process consisting of DC magnetron sputtering of composite Cu-In-Al metallic precursors, followed by selenization in an Ar and Se atmosphere. All precursor layers were sputtered from composite targets with fixed stoichiometric ratios of $Cu_{0.45}In_{0.55-y}Al_y$ (y = 0.05, 0.15, 0.25, 0.35, 0.45, 0.55). Prior to deposition the chamber was evacuated to a base pressure of 1×10^{-4} Pa with a turbo molecular pump. High purity (99.998%) Ar was used as the working gas. The argon flow rate was set to 40 sccm for all samples and the total deposition time was approximately 30 minutes. A deposition rate of 15 nm/min produced thin films with thicknesses near 450 nm before selenization. (After selenization the thickness approximately doubled.) A set of 6 samples with initial ratio *x* = Al/(In+Al) = 0.09, 0.27, 0.46, 0.64, 0.82 and 1 was prepared.

All samples were selenized in a quartz halogen lamp heating system using a solid pure selenium source (Alfa Aesar, purity: 99.999+%). A computer was used to control the temperature profile during the experiment. Because formation of CIAS starts at a temperature of 490 °C [3], the final selenization temperature was set to 550 °C. The temperature profile during selenization was the following: a one step ramp and soak process with a 5 minute ramp directly to the final temperature 550 °C followed by a 60 minute soak and controlled cool down to return the container to room temperature. The total reaction time was 65 min.

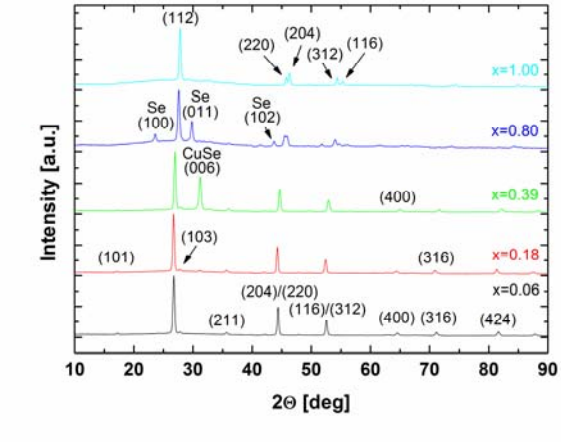

Figure 5. XRD patterns of CIAS samples selenized in an Argon atmosphere with Se vapors at 550°C for 60 minutes.

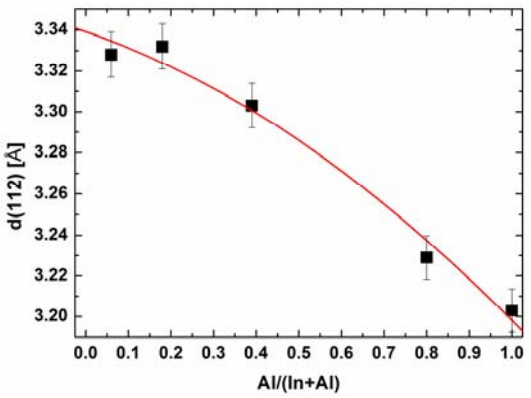

Figure 6. Variation in lattice spacing d(112) of CIAS thin films with the Al/(In+Al) ratio.

XRD patterns of CIAS samples selenized under a one step process are shown in Figure 5. From these patterns, it is observed that all the films are polycrystalline in nature. The presence of weak peaks such as the (101), (103), and (211), and especially the well resolved doublet-peaks (220/204) and (312/116), which appear for high values of the parameter *x,* confirm that the structure is chalcopyrite. Some unwanted phases are

presented in the spectra of samples with x = 0.39 and 0.80. These phases were identified as hexagonal crystals of CuSe (See also the hexagonal plates in SEM images - Fig. 7b) and pure Se crystallizing in space group P3_221. A significant shift of all peaks to higher 2θ positions is observed with increasing Al ratio due to a decrease in d-spacings and unit cell dimensions. The dependence of lattice spacing d(112) on Al content is shown in Figure 6. The lattice parameters *a* and *c* were calculated from peak positions corresponding to reflections (112), (204) and (312). Their values varied in the range 5.59 Å to 5.77 Å for *a* and 10.95 Å to 11.56 Å for *c,* and it seems that their dependence on Al content is nonlinear. The similar deviation from the Vegard's law for CIAS thin films has been reported also in some previous work [4-6]. The tetragonal distortion (2-*c*/*a*), which is an important parameter in chalcopyrite compounds, is almost zero for $CuIn_{1-x}Al_xSe_2$ with a low value of the parameter x and significantly grows with the increase in Al concentration. This fact could be indicative of tension in a crystal structure and therefore on the crystallite size.

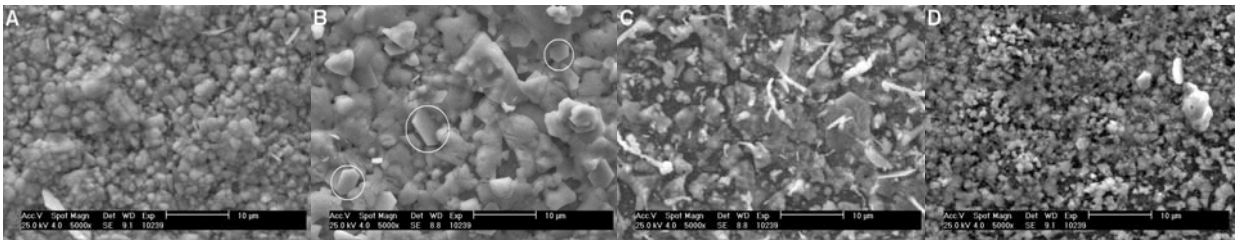

Figure 7. SEM images of $CuIn_{1-x}Al_xSe_2$ thin films with A) x = 0.18 B) x = 0.39 C) x = 0.80 and D) x = 1.00. White circles in Figure 5B represent unwanted CuSe hexagonal crystals.

The SEM images of four selected samples with x = 0.18, 0.39, 0.80 and 1.00 are presented in Figure 7a–d respectively. They reveal that more homogeneous distribution is exhibited by the samples with low x or with x close to 1. Samples with x around 0.5 revealed some of the unwanted phases and impurities such as $Cu_{2-x}Se$ and pure un-reacted Se. For example, in Figure 7b, it is possible to see hexagonal plates of CuSe crystals (the encircled areas), which were also identified in the XRD and Raman spectra. The easily visible white nanorods in Figure 7c represent the rest of the selenium that did not react with precursors. An excess of selenium was also confirmed by ICP-MS in all samples regardless of Al content and is probably a consequence of the temperature drop at the end of the selenization process. Unreacted selenium in Se vapor condensed in an Ar atmosphere on the surface of each sample immediately when the temperature drops below 221°C. Another unwanted effect that was noticed after the selenization procedure was a significant loss of Al. Before selenization the Al/(Cu+In+Al) ratio was 0.05, 0.15, 0.25, 0.35, 0.45 and 0.55 after selenization this ratio was almost 30% lower. A similar effect with Al loss was reported in a previous paper [1].

The Raman spectra of $CuIn_{1-x}Al_xSe_2$ thin films were recorded at room temperature and the results are presented in Figure 8. The A_1 phonon frequency reveals a significant shift with the increase of Al/(In+Al) content from 172 cm^{-1} (A_1-mode frequency of $CuInSe_2$) to 186 cm^{-1} (A_1-mode frequency of $CuAlSe_2$). The final shift is in good

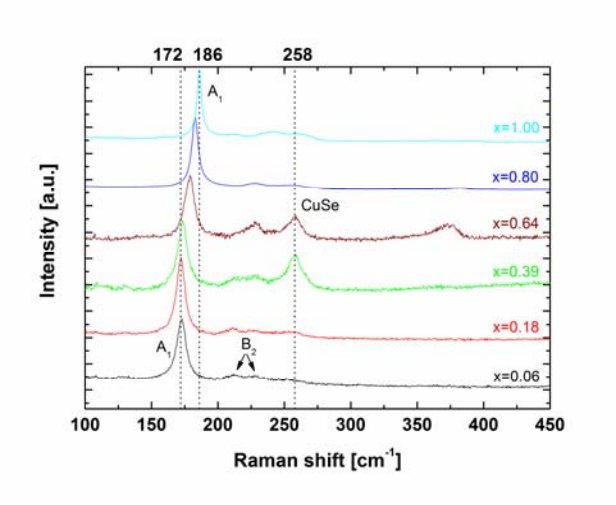

Figure 8. Raman spectra of CIAS samples selenized in an Argon atmosphere with Se vapors at 550°C for 60 minutes.

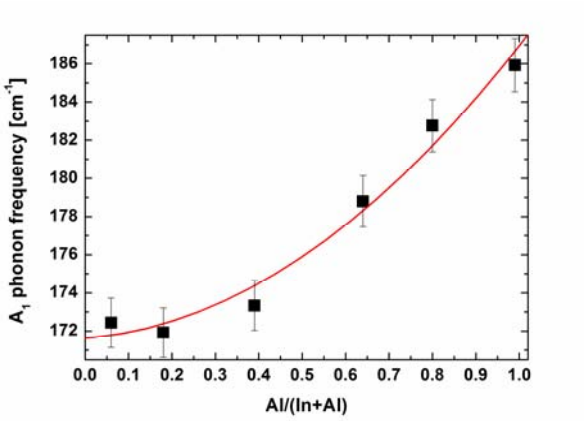

Figure 9. A_1 phonon frequency as a function of Al content.

agreement with all known previous published studies focused on Raman spectroscopy of $CuAlSe_2$ material [7-11]. From Figure 9 it can be seen that for $x < 0.4$ the shift of the A_1 band is negligibly small and as well as the lattice constants *a* and *c,* or plane spacing *d,* does not follow the linear Vegard law.

For a sample with $x = 0.64$, sequential formation of In_xSe_y, $Cu_{2-x}Se$, CIS and CIAS phases was observed from temperature resolved Raman spectra, and conversion of CIS to CIAS was initiated at 500°C. Dual phase formation was observed in samples with an Al/(In+Al) ratio close to 0.5.

One other nanocrystal-to-thin-film processing method that was explored was the preparation of a quaternary chalcopyrite sulfide precursor followed by the reaction with selenium to form the chalcopyrite selenide. Guo *et. al.* [12] have demonstrated that a dense thin film of chalcopyrite-phase $CuInSe_{1.8}S_{0.2}$ may be prepared by reaction of H_2Se gas with a film cast from a $CuInS_2$ nanoink suspension. Replacement of the S^{2-} ions with the larger Se^{2-} ions reduces void formation and device efficiencies as high as 5.55% have been reported [12]. In selenization reactions such as this, atmospheres of excess H_2Se or Se vapor are typically maintained over the $CuIn_{1-x}Ga_x$ alloy films in order to generate CIGS films of uniform composition. While we were unable to prepare stable $CuIn_{1-x}B_xS_2$ nanoparticles to serve as CIBS precursors, this route was studied for the preparation of $CuIn_{1-x}Ga_xSe_2$ (CIGS, x = 0, 0.25, 0.5, 0.75, 1) **with the novel aspect that the only source of Se in the second reaction was a layer of colloidal Se particles sprayed on the $CuIn_{1-x}Ga_xS_2$ nanoparticle precursor** [13].

Nanoink suspensions of $CuIn_{1-x}Ga_xS_2$ in toluene were prepared as described in the literature [12]. A colloidal Se spray solution was prepared by complexing Se with a condensation product of ethylenediamine (EDA) and 2,2-dimethylimidizolidine. A mixture of 2,2-dimethylimidizolidine (10.0 mL), EDA (9.1 mL), and toluene (5.7 mL) was refluxed at 85 °C for 2 hours. The resulting condensation product (20.0 mL) was

collected in a Dean-Stark trap and a portion (6.0 mL) was combined with EDA (4.1 mL) and Se powder (200 mesh, 0.3959 g). This mixture was refluxed with stirring for one hour. After cooling to room temperature, a 2-mL portion was combined with 40 mL of 2-propanol that had been heated to 45 ^{o}C for 30 minutes. Within one minute, the resulting mixture turned a brilliant red color indicative of colloidal Se formation.

Films of Se and $CuIn_{1-x}Ga_xS_2$ were squentially sprayed onto a heated (120 ^{o}C) plain or Mo-coated sodalime glass microscope slide at a rate slow enough to allow the solvent to evaporate immediately on contact with the slide. The $CuIn_{1-x}Ga_xS_2$ nanoink suspension was sprayed by airbrush onto the Se-coated slide in a vertical position until a 1:2 mole ratio was achieved as determined by weighing the sample after solvent evaporation. In some samples on Mo-coated slides, the $CuIn_{1-x}Ga_xS_2$ and Se were spray-deposited in reverse order.

To prepare a $CuIn_{1-x}Ga_xSe_2$ (x = 0, 0.25, 0.5, 0.75, or 1) film, the $CuIn_{1-x}Ga_xS_2$/Se coated slide was placed in a graphite container. This was loaded into a quartz tube that was evacuated to a base pressure of less than 1 Pascal and then filled with 1 atm of argon (99.999%). A thermocouple was inserted into the body of the graphite container heated for 60 minutes at 550°C.

Upon heating the dual-layered Se/$CuIn_{1-x}Ga_xS_2$ precursor films at 550 ^{o}C for one hour in a 1-atm argon atmosphere, the Se diffuses through the $CuIn_{1-x}Ga_xS_2$ layer, displacing the sulfur to form the final CIGS product. XRD patterns of the product $CuIn_{1-x}Ga_xSe_2$ films (Figure 10) are consistent with the chalcopyrite unit cell and show diffractions from the (112), (220/024), and (116/132) planes. All peak positions shift toward higher 2θ values as the Ga/(In+Ga) ratio increases. Calculated lattice parameters change nearly linearly between those for $CuInSe_2$ (a = 5.791 Å, c = 11.585 Å) and $CuGaSe_2$ (a = 5.637 Å, c = 10.992 Å) as shown in Figure 11.

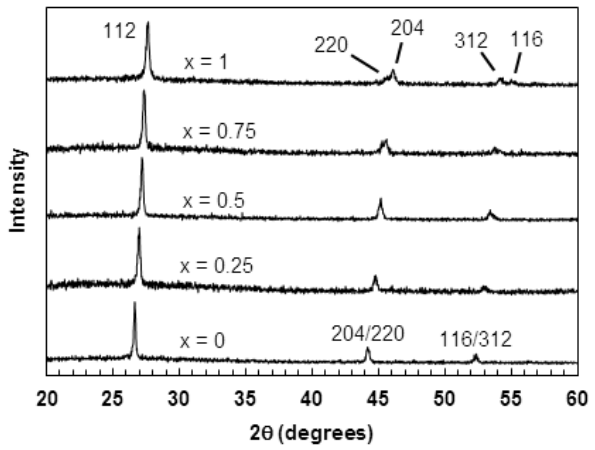

Figure 10. XRD patterns for product $CuIn_{1-x}Ga_xSe_2$ (x = 0, 0.25, 0.50, 0.75, 1) films.

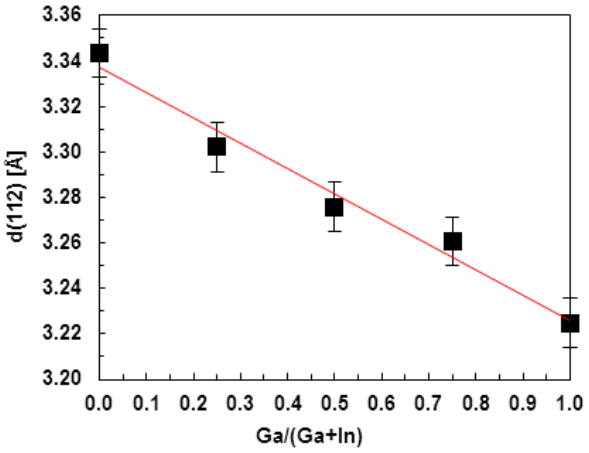

Figure 11. (112) lattice plane spacing (Å) as a function of Ga/(Ga+In).

Raman spectra show a similarly linear shift in A_1 phonon frequency between that for $CuInSe_2$ (171 cm^{-1}) and $CuGaSe_2$ (184 cm^{-1}) as seen in Figure 12. No residual $CuIn_{1-x}Ga_xS_2$, $Cu_{2-x}Se$, or $Cu_{2-x}S$ phonon signals are present and these XRD and Raman data indicate that all sulfur may have been displaced from the films. SEM images (Figure 13) of $CuIn_{1-x}Ga_xSe_2$ films show grains that are 200-300 nm in diameter and comparable in size to the $CuIn_{1-x}Ga_xS_2$ precursor nanoparticles.

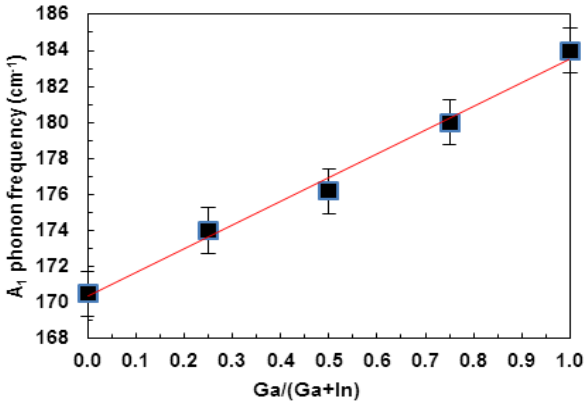

Figure 12. A_1 phonon frequencies for product $CuIn_{1-x}Ga_xSe_2$ films as a function of Ga/(Ga+In)

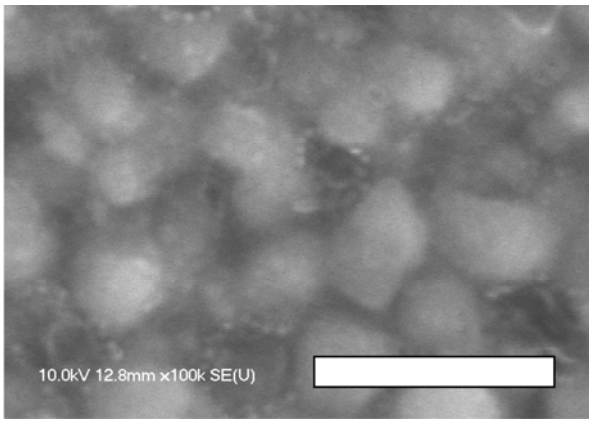

Figure 13. SEM image of product $CuInSe_2$ film (white scale bar = 1.00 μm)

When excess $CuInS_2$ was used, Cu-rich CuAu-ordered $Cu_{1.5}InSe_2$ phase resulted. The additional copper shifted the $CuInSe_2$ A_1 phonon frequency that typically appears at about 173 cm^{-1} to about 175 cm^{-1} and broadened the peak with a shoulder at 183 cm^{-1}, a peak characteristic of the copper rich $Cu_{1.5}InSe_2$ phase [14].

In working toward the fabrication of a PV device prototype, the layering of nanocrystalline $CuInS_2$ and colloidal Se on Mo-coated sodalime glass substrates was attempted. Repeating our previous layering order ($CuIn_{1-x}Ga_xS_2$/Se/Mo-SLG) and heating procedures resulted in $MoSe_2$ as the primary film product. It was necessary to reverse the layering order (Se/ $CuIn_{1-x}Ga_xS_2$/Mo-SLG), lower the reaction temperature to 500 ^oC and shorten the reaction time to 45 minutes in order to produce CIGS films with nominal Ga/(Ga+In) ratios that have been characterized by Raman spectroscopy.

Raman spectra (Figure 14) showed a linear shift in A_1 phonon frequency (Figure 15) between that for $CuInSe_2$ (171 cm^{-1}) and $CuGa_xSe_2$ (184 cm^{-1}). No residual $CuInS_2$, $CuGaS_2$, $Cu_{2-x}Se$, or $Cu_{2-x}S$ phonon signals are present, indicating that all sulfur may have been displaced from the films.

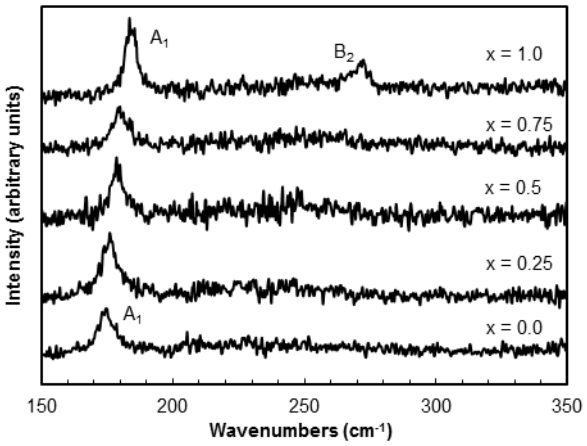

Figure 14. Raman spectra of $CuIn_{1-x}Ga_xSe_2$ (x = 0.0, 0.25, 0.50, 0.75, 1.0) thin films prepared on Mo-coated sodalime glass.

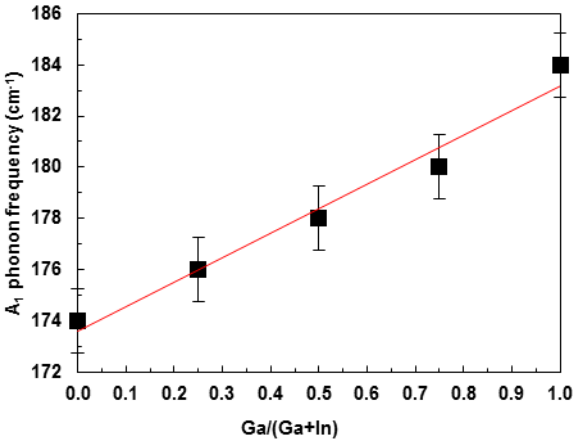

Figure 15. A_1 phonon frequency of $CuIn_{1-x}Ga_xSe_2$ (x = 0.0, 0.25, 0.50, 0.75, 1.0) thin films on Mo-coated sodalime glass as a function of Ga/(Ga+In) ratio.

Task 2.0 [Preparation of Thin-Film CIBS using in-situ Selenization].

Our previous studies of *ex-situ* selenization of $CuIn_{1-x}B_x$ thin films concluded that boron segregated from Cu, In, and Se during film formation [15]. In this project, an *in-situ* selenization system was developed. The proof-of-principle was demonstrated by the *in-situ* $CuInSe_2$ (CIS) deposition process. By depositing CuIn in a Se-rich atmosphere we produced CIS films that were verified by AES (Figure 16) and XRD (Figure 17). A post-anneal process was required to improve the films' transmission coefficient. The Tauc bandgap was estimated to be 1.07 eV.

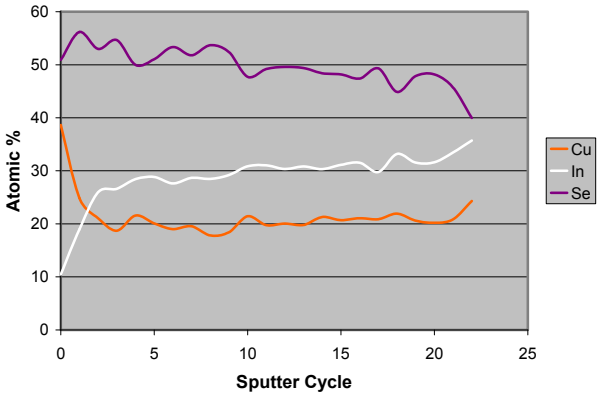

Figure 16. AES depth profile of an *in-situ* selenized $CuInSe_2$ film.

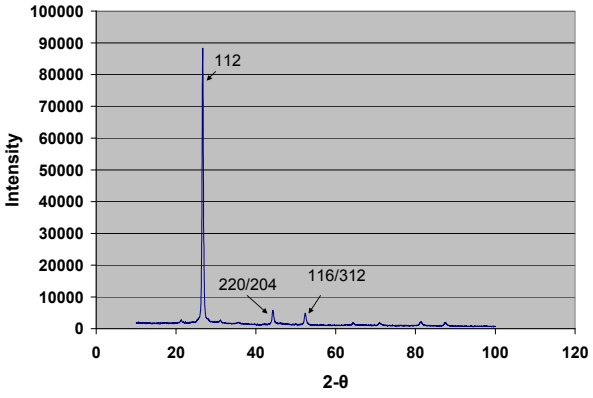

Figure 17. X-ray diffraction results for an *in-situ* selenized $CuInSe_2$ film

Efforts to deposit $CuIn_{1-x}B_xSe_2$ films encountered complications. The CuInB target purchased for deposition of CIB precursors and *in-situ* deposited CIBS thin film absorbers was discovered to be B-deficient on the surface. After several attempts at producing a CIB target they realized that they could not fabricate the material with uniformity of elements. Thus, they fabricated a CuB target that was sputtered along with a CuIn target. $Cu_{.45}In_{.55-x}B_x$ precursor films of varying boron concentration (22-63%) were deposited on molybdenum coated stainless steel in order to facilitate higher selenization/sulfurization temperatures. Selenization/sulfurization temperatures of 550, 650, and 750 C were used. In all cases, the resultant films peeled off the substrate or did not form the desired chalcopyrite with incorporated boron. The experiment was repeated with just a $Cu_{.45}B_{.55}$ film onto quartz in order to attain the higher temperatures. These films remained adherent and appeared to have a wide bandgap because they are transparent; however, chemical analyses revealed that CIBS had not been produced.

Expertise gained from these and previous *ex-situ* selenization studies was applied to new studies in the preparation of thin-film pyrite FeS_2, an attractive earth-abundant candidate material for next-generation photovoltaics. In recent years, iron disulfide has attracted considerable attention as a candidate for alternative solar cell materials. The very high absorption coefficient, $\alpha = 6 \times 10^5$ cm^{-1} for $\lambda = 633$ nm [16] and the composition of abundant, cheap and non-toxic elements makes pyrite an interesting material for thin-film solar cells [17]. Iron disulfide has a bandgap energy of $E_g = 0.95$ eV, [18] somewhat less than the ideal. However, a thorough modeling of the potential of pyrite indicates that efficiencies of 20% are possible [19]. Despite these favorable physical properties, the conversion efficiencies of pyrite thin film solar cells have been disappointing and an incentive for further study.

In our studies, three methods successfully produced pure pyrite FeS_2 films: sulfurization of sputtered Fe films, chemical bath deposition, and sulfurization of Fe_2O_3 sol-gel precursors..

Growth of FeS_2 thin films by DC sputtering method: Fe films were obtained by DC sputtering of Fe onto soda lime glass substrates at ambient temperature. The thickness of the as-grown Fe films ranged from 200 to 300 nm. In order to fabricate pyrite, the Fe films were sulfurized in an open glass quartz ampule and annealed at different temperatures in a sulfur and nitrogen atmosphere for 1 hour.

Figure 18 shows the sequence of X-ray diffraction patterns of as-grown Fe film and films formed after sulfurization at different temperatures. FeS_2 (pyrite) and FeS (monoclinic) XRD signal positions fromm the standard ASTM cards are shown for comparison. As can be seen, pyrite films are clearly obtained at annealing temperature of 350°C and 450°C. XRD patterns gave no indication of other phases such as pyrrhotite, FeS, sulfur or iron. In case of annealed at 450°C temperature the XRD peaks had very strong reflection peaks.

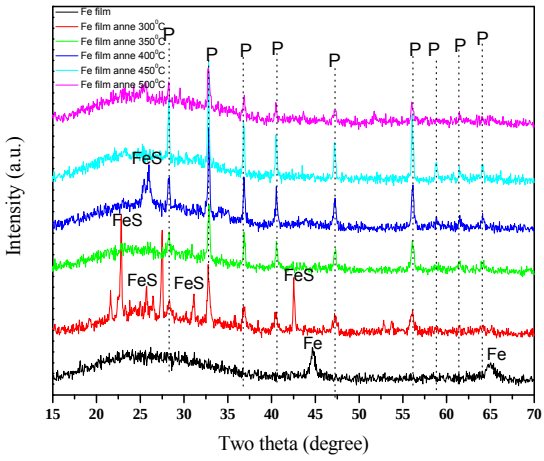

Figure 18. XRD pattern of DC-sputtered Fe films before (black) and after annealing at 300 (red), 350 (green), 400 (dark blue), 450 (light blue), and 500 ^{o}C (pink).

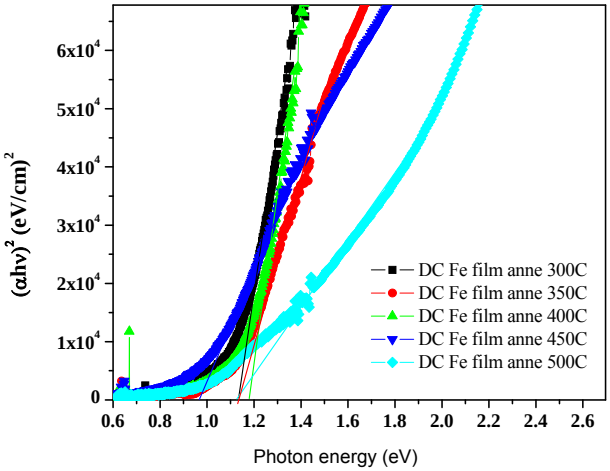

Figure 19. $(\alpha h\nu)^2$ versus $h\nu$ for FeS_2 films annealed at 300 (black), 350 (red), 400 (green), 450 (dark blue), and 500 ^{o}C (light blue).

Figure 19 shows the plots of $(\alpha h\nu)^2$ vs $h\nu$ of films after sulfurization at different temperatures. In this figure the apparent $(\alpha h\nu)^2$ versus $h\nu$ is plotted. α is determined from reflection and transmittance spectra. The optical bandgap for the film annealed at 450°C is approximately 0.96 eV, as expected for FeS_2. We found that the FeS_x thin films were all of p-type conductivity regardless of annealing temperature.

Growth of FeS_2 thin films by the chemical bath deposition method: FeS_2 layers were deposited on soda lime glass. The deposition bath consisted of an aqueous solution containing $FeSO_4$, $Na_2S_2O_3$•$5H_2O$, ethylenediamine and methanol. Initially 3ml of 1M $FeSO_4.7H_2O$ solution to which 20ml of the double distilled water was added and stirred for 15 minutes. After that one drop of ethylenediamine solution in 10ml of methanol was added. The solution immediately changed from in color light green to dark green and was vigorously stirred for 15 minutes. Finally 10ml of $Na_2S_2O_3$•$5H_2O$ solution was added to bring up the total volume of the mixture to 50ml. The temperature of the bath was kept at room temperature and the deposition time was 20 hours. The substrates were taken out of the chemical bath, rinsed with toluene and allowed to dry. The annealing treatment was performed in an open quartz tube in nitrogen and sulfur atmosphere for 1 hour. Sulfurization temperatures between from 350°C to 550°C were used in our experiments.

SEM images of the as-deposited and annealed (450°C) pyrite samples are shown in Figure 20.

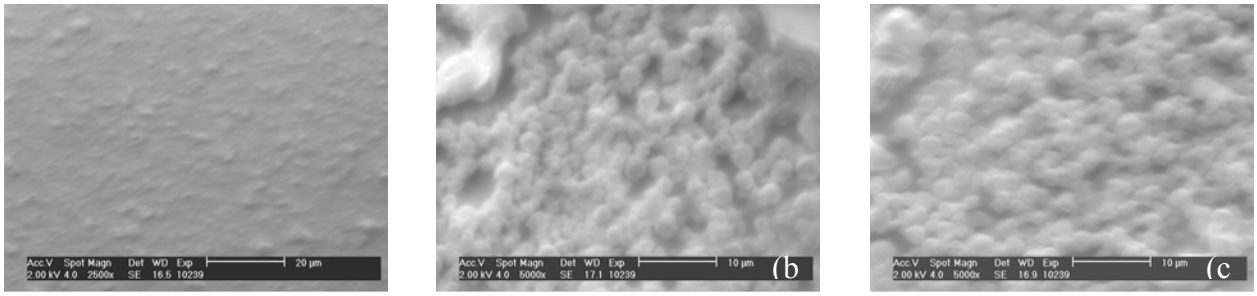

Figure 20. SEM images of (left) as-deposited and (middle, right) annealed (450 °C) FeS_2.

Figure 21 shows X-ray diffraction (XRD) resultsThe as-deposited film shows no diffraction peaks, illustrating that it is amorphous. The patterns for the samples heated at 350 °C and 400 °C for one hour in the nitrogen and sulfur atmosphere shows that the material is a mixture of iron sulfide phases, including pyrite. Annealing at 450 °C brings about the formation of the single crystalline pyrite phase without any contributions from other phases. The (200) plane appears to be the preferred orientation of the pyrite crystallites. In the case of processing at 550 °C, the sample shows a mixture of iron sulfide phases, including marcasite and pyrrotite phases that may result from the decomposition of the pyrite.

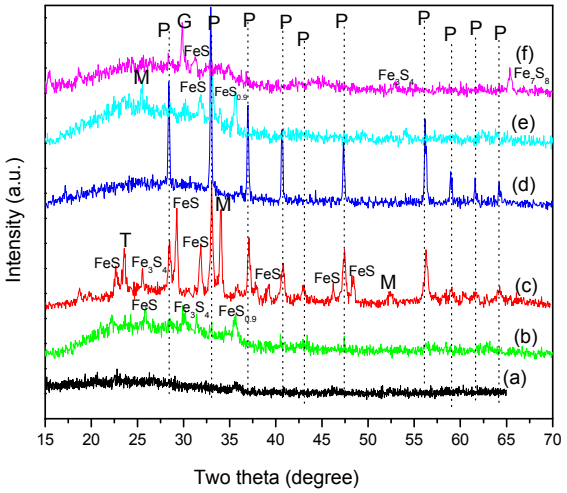

Figure 21. XRD of the as-deposited and processed films under different temperatures (a) as-deposited (b) 50°C (c) 400°C (d) 450°C (e) 500°C (f) 550°C, [P =Pyrite (FeS_2), M=Marcasite (FeS_2),G=Greigite (Fe_3S_4), T=Troilite (FeS) and FeS-P =Pyrrhotite (FeS)].

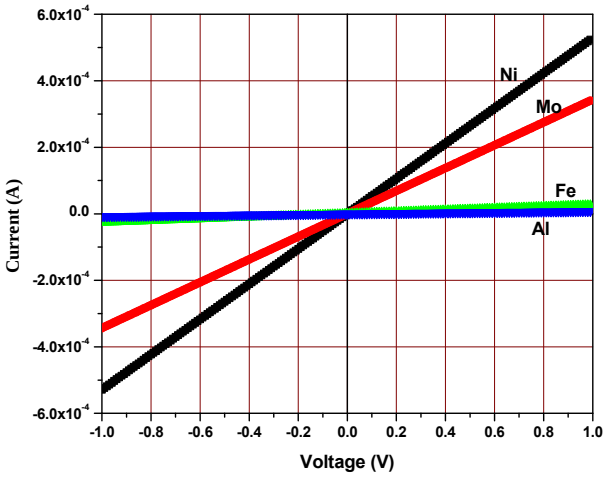

Figure 22. Linear I-V characteristics of the FeS_2 – metal contacts, Al, Mo, Fe, and Ni,illustrating that Ni yields the lowest resistance ohmic contact.

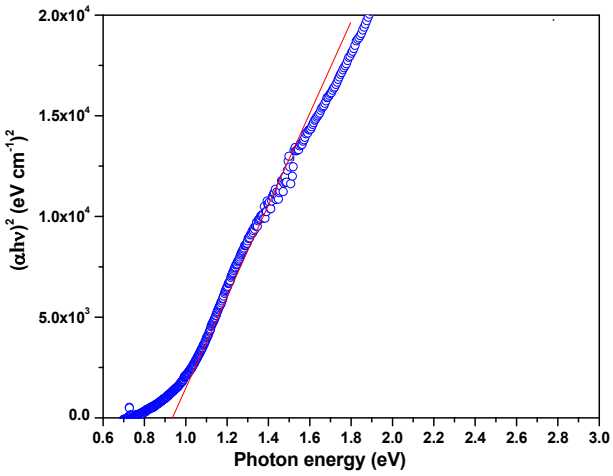

Figure 23. $(\alpha h\nu)^2$ vs $h\nu$ for the film sulfurized at 450 °C for 1 hour.

It has been shown by Schieck, et.al. [20] that platinum makes a very good ohmic contact to p-type iron pyrite, where Cu and Au both exhibited non-linear current-voltage characteristics and Al and Pt were linear at currents in the mA range. In search of a good ohmic contact material that is less expensive that Pt, the following metals were chosen for study: Al, Mo, Fe and Ni. Current-voltage characteristics of these metals on pyrite FeS_2 thin films are shown in Figure 22. Although each metal produced a linear current-voltage characteristic, Ni was seen to be the best with a resistance of about 2 kΩ. This resistance was further lowered when in contact with pyrite films formed from sulfurization of sputter-deposited Fe thin films. Electrical resistivity measurements were made using the van der Pauw method. The resistivity of p-type pyrite thin films were 54.57 Ωcm and 18.45 Ωcm, depending on grain size.

Figure 23 shows the optical absorption spectrum for this thin film sulfurized at 450 ^{o}C for 1 hr. The film processed at 450 °C had an apparent bandgap of 0.94 eV that is in agreement with the literature [18].

Preparation of FeS_2 thin films by the sol-gel method: Iron oxide thin films were synthesized according to the following procedure. Iron(III) nitrate (2.5 g) was dissolved in ethyl alcohol (10 ml) and used as a molecular precursor of Fe_2O_3. Then, 2 ml of propylene oxide was dropped slowly into the solution and after a few minutes the solution turned dark. The prepared solution was used to spin coat previously cleaned sodalime glass substrates at 2200 rpm. By a single spin, thin (~ 50 nm) layers were obtained; whereas thicker layers were obtained by multiple coatings. After each spin coating, thermal treatments were performed raising the temperature at approximately 100 °C/h and keeping the temperature at different levels for 1 hour.

The calcinated layers were sulfurized in an evacuated quartz tube using a Rapid Thermal Annealing (RTA) irradiation lamp as a heating source. During the sulfurization, the samples were kept in a graphite boat together with sulfur powder. The sulfur amount of 1 g was the same for all the experiments. The boat was placed in the quartz tube, in which it was connected via a thermocouple to a station operating the RTA lamp. The tube was first evacuated and then filled with Argon. The temperature was increased at the rate of 150 °C/ min up to 450 °C. At this temperature level, the samples dwelled for 15 minutes and then the RTA was turned off allowing the temperature to decrease slowly to ambient temperature. The influence of two parameters, temperature and time of sulfurization, was studied. The sulfurization temperature was varied between 400 °C and 500 °C (heating rate 150 °C/ min, 1 hour dwelling time in these experiments) and the sulfurization time was constantly decreased from 5 hours to 15 min at the temperature of 450 °C, the temperature which yielded the best results.

The sol-gel method appeared to be a suitable candidate for the production of high-quality pyrite layers. Figure 24 shows the Raman spectrum of a five-layer α–Fe_2O_3 coating after sulfurization at different temperatures.

The best result, in terms of achieving the desired pyrite crystal phase, was accomplished by performing the sulfurization at 450 °C. It is known that at this temperature, sulfur is in its cyclic S_8 form, which is the most suitable for the sulfurization processes. Three basic Raman bands of pyrite, corresponding to the peaks at 339 cm^{-1}~ E_g, 374 cm^{-1}~ A_g and 426 cm^{-1}~ T_g, were observed in the spectrum (see Fig. 1). The complete chemical transformation from the hematite to pyrite was achieved after 15 minutes. This is a very appealing condition for potential solar cell fabrication.

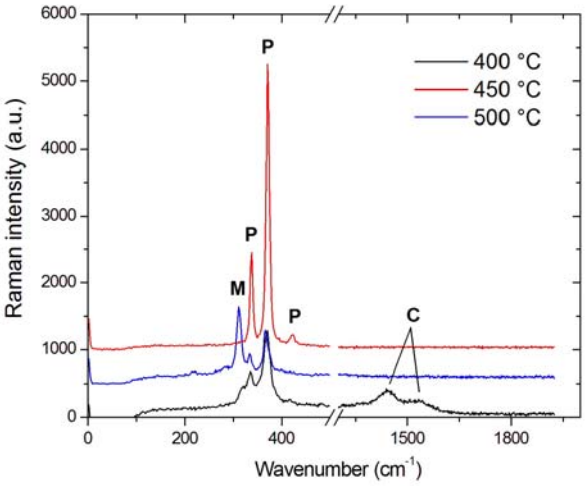

Figure 24. Raman spectra of FeS_2 films sulfurized at different temperatures for one hour. In the graph, P - Pyrite, M – Marcasite and C – Carbon.

SEM images of the samples can be seen in Figure 25. It is evident that increasing the time of sulfurization led to the formation of larger grain aggregates, which resulted in films' greater roughness. Nevertheless, no significant defects in the films were detected.

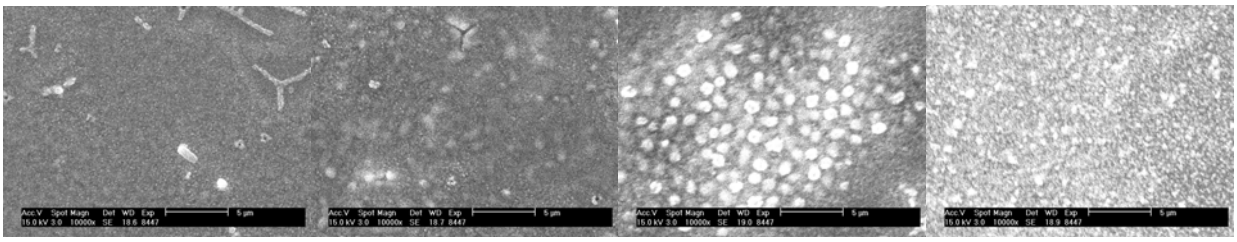

Figure 25. SEM images of the samples sulfurized at 450 °C for: (left to right) 15 min, 1 h, 3 h and 6 h.

XRD analyses correlate with the Raman spectroscopy data. Only pyrite phase diffraction signals were observed and peak intensities were almost equal for all time durations, indicating the same extent of crystallization (Figure 26).

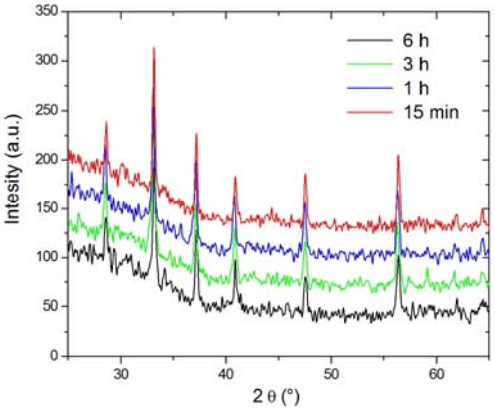

Figure 26. XRD spectra of pyrite films prepared by sulfurizations of varying time duration.

The sample with five successively deposited layers is of interest because its thickness is in the appropriate range for photovoltaic applications. This film was annealed five times (once after each spin coating) at 600 °C to achieve the hematite structure and further sulfurized at 450 °C for 15 minutes. Na contamination was encountered in these films of several layers. The more times the sol-gel material was annealed the more likely the

Na was diffusing from the soda lime glass into the film. Glow discharge optical emission spectroscopy (GDOES) showed considerable penetration of the Na into the FeS_2 (see Fig. 5). This problem is being studied by using various barrier coatings and different substrates.

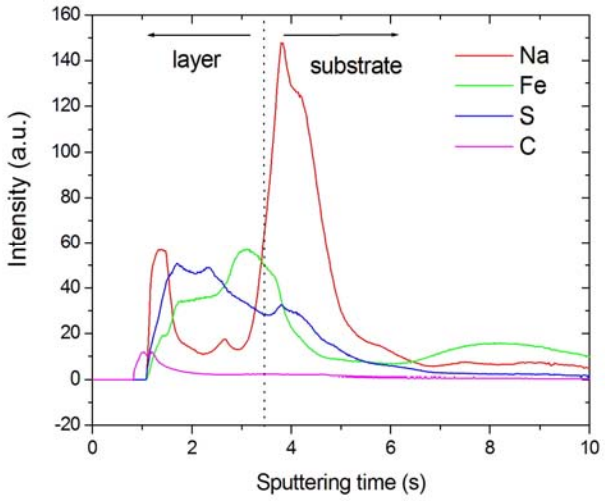

Figure 27. GDOES elemental depth profile of the film sulfurized for 15 min at 450 °C.

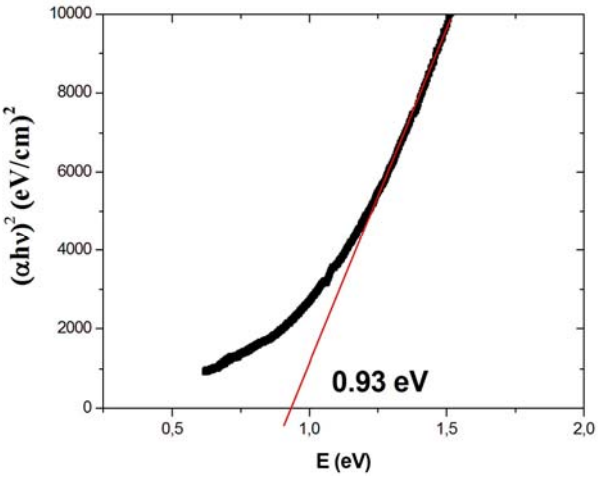

Figure 28. Tauc plot of the film sulfurized for 15 min at 450 °C. The intersection of the red line with energy axis denotes the band gap energy.

Auger scans of the films revealed that the stoichiometry of the film was almost precisely 2 (S):1 (Fe), within the range of precision of the AES system and was constant through the entire film. The band gap energy determined form the Tauc measurement (Figure 28) was 0.93 eV, which is just slightly below the expected value of 0.95 eV [18].

The photo-responses of the films were assessed using photoelectrochemical amperometry. For this purpose, the layered system of conductive (Indium doped tin oxide) ITO substrate / anatase TiO_2 / FeS_2 was prepared. The system was illuminated with light corresponding to band gap of FeS_2., which served as the prime absorber sensitizing the anatase film. The system is conventional three electrode set-up of a working electrode ($ITO/TiO_2/FeS_2$), auxiliary electrode (Pt) and a reference electrode (Ag/AgCl in 3M KCl).

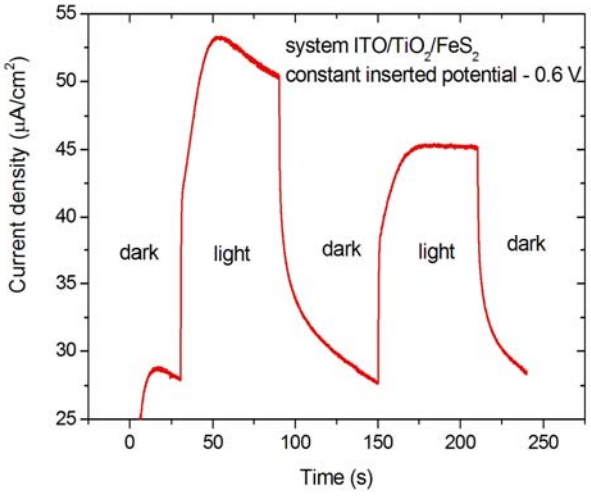

Figure 29. Photocurrent curve – dependency on time at fixed potential of 0.6 V.

Figure 29 shows the dependence of current density (photocurrent) on time under a fixed potential of 0.6 V. The rather low value of the photocurrent is probably due to the high recombination rate of the carriers (electron/hole pair) and sulfur deficiencies in the lattice.

As described earlier, we have shown that in addition to Pt, the inexpensive metal, Ni, makes a good ohmic contact to iron pyrite. However, it was discovered that during the sulfurization of the hematite, that the Ni also reacted with the sulfur, forming nickel sulfide. Thus, a search for a buffer layer or a new ohmic contact was initiated.

SnS_2 Thin Films as a Potential Heterojunction Partner for FeS_2. To the best of our knowledge, heterojunction solar cells with SnS_2 as the window layer and FeS_2 as the absorber have not been investigated to date. As with any heterojunction device, the band alignment is critical and this is especially true for solar cells. A literature study of transparent conducting materials has revealed that SnS_2 may be a suitable window layer/heterojunction partner for an iron-pyrite (FeS_2) collector. It is n-type and its band gap is reported to be in the range of E_g = 2.12-2.44 eV [19], depending on type, alpha or beta, and is therefore transparent to photons of interest. The electron affinity of SnS_2 is reported to be χ = 4.2 eV [19], while that for FeS_2 is reported to be in the range of χ = 3.9 eV [7] to χ = 4.5 eV [18]. If the interface states at the FeS_2 /SnS_2 interface can be ignored, i.e., minimized, band diagrams such as seen in Figure 30 could result. It can be seen that, if the electron affinity of FeS_2 is at the upper end of the scale the collecting junction will have a blocking barrier for the collection of minority electrons, Fig. 7 (left), however, if at the lower end of the scale, Figure 30 (right), this combination has the potential of being a good electron collection junction. Since both Fe and Sn bond preferentially with two S atoms, it is quite likely that a graded transition in the junction region can be developed and the spike in the conduction band, if it exists, can be eliminated that way.

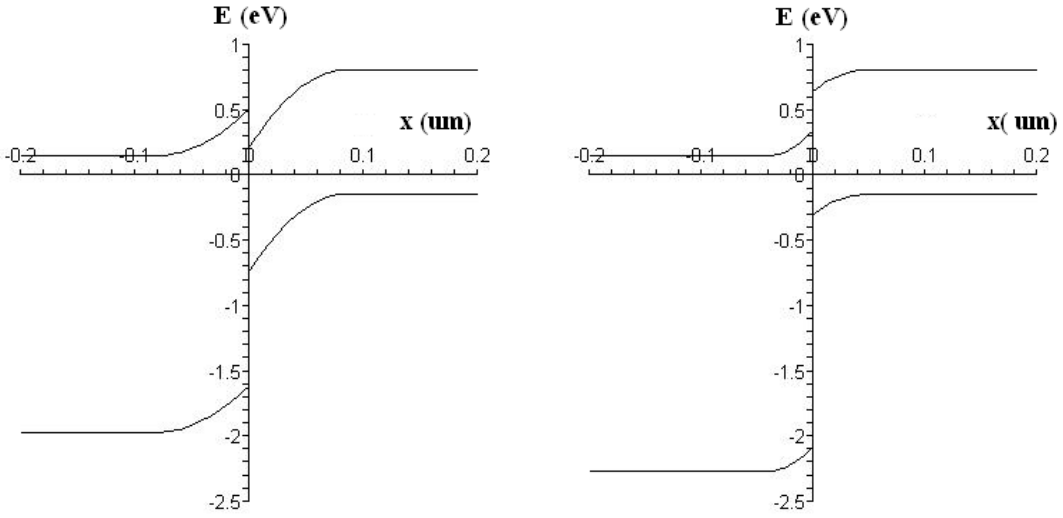

Figure 30. Possible band diagrams for FeS_2 couples with (left) SnS_2 if the electron affinity of FeS_2 equals 4.5 eV, (right) SnS_2 if the electron affinity of FeS_2 equals 3.9 eV.

Thin Sn films of 100 nm thickness were sputtered onto the soda lime glass using DC magnetron sputtering. The films were then heated in a sulfur and nitrogen atmosphere. Sulfurization was done either as a 1-step process or a 2-step process. In the 1-step process, the oven was heated to the desired temperature and the Sn film was loaded into a carbon boat with 0.7 g sulfur, placed into the oven for 1 hour and then cooled under nitrogen flow until it reached 45°C. In the 2-step process the procedure was repeated on the same sample at a higher temperature.

It was observed that the tin film initially formed blue-colored SnS at lower temperatures and formed yellow-colored SnS_2 at higher temperatures. Figure 31 shows the XRD patterns of the Sn film after sulfurization as a function of temperature. It is clear that the film is mostly tin at 170 °C and starts to form SnS at 200°C, the maximum intensity of a singular signal being at 250 °C. The best film for SnS_2 was obtained at 350 °C. Figure 31 highlights the compounds and the corresponding planes as found from the powder diffraction tables for Sn, SnS, and SnS_2.

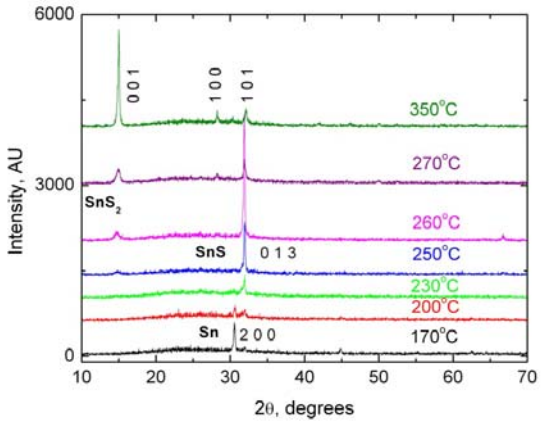

Figure 31. X-ray diffraction (XRD) patterns for Sn film after sulfurization under different conditions. The spectra identify Sn sulfurized by one-step process at the labeled temperatures.

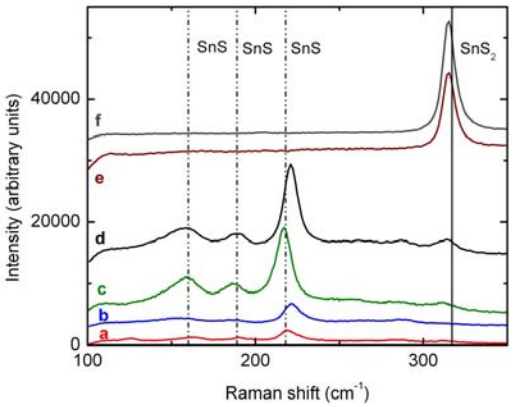

Figure 32. Raman spectra for Sn film after sulfurization under different conditions. The dotted vertical lines denote peaks for SnS whereas the solid vertical lines denote peaks for SnS_2. The spectra identify Sn sulfurized in one-step for 1 hour at (a) 170°C (b) 200°C (c) 250°C; sulfurized in two steps for 1 hour at (d) 250°C and 300°C (e) 250°C and 350°C ; and (f) heating from room temperature to 350°C and sulfuring at 350°C for 1 hour.

The study of SnS_2 formation as a function of time shows that the film can be formed within 15 minutes of annealing. Figure 32 shows the Raman spectra for Sn film after sulfurization under various conditions. The dotted vertical lines denote the peaks identifying SnS and solid vertical line denotes the peak identifying SnS_2 [21]. It is noteworthy that the peaks for SnS start to appear when the sulfurization is accomplished at 170°C and they increase in intensity as the temperature is increased. The SnS peaks then decrease while the peak intensity for SnS_2 increases. Thus it can be inferred that Sn is first sulfurized to form SnS and then SnS_2. The strongest intensity

for SnS_2 is obtained when the Sn film was heated from room temperature to 350°C and annealed at 350°C for 1 hour. From Figures 31 and 32 it can be inferred that the best SnS_2 films are obtained when heating the Sn film to 350°C and sulfurizing for 15 minutes to one hour. The sample which has the most intense (001) XRD peak for SnS_2 also has the most intense peak for a Raman shift at near 317 cm^{-1}.

Figure 33 shows the Tauc plots for Sn films sulfurized under various conditions. In this Tauc plot $(\alpha hv)^2$ is plotted vs. hv to determine the bandgap. The bandgap measured for SnS was 1.61 eV and bandgap for SnS_2 is found to be 2.52 eV. This is similar to the findings of Sugiyama, *et. al.* [22,23] and Thangaraju and Kaliannan [24] for SnS and SnS_2 respectively. From the Tauc plot, it is also evident that SnS_2 is formed in a two stages, viz. Sn is sulfurized to SnS and then SnS_2, thereby corroborating the results obtained by XRD and Raman Spectroscopy.

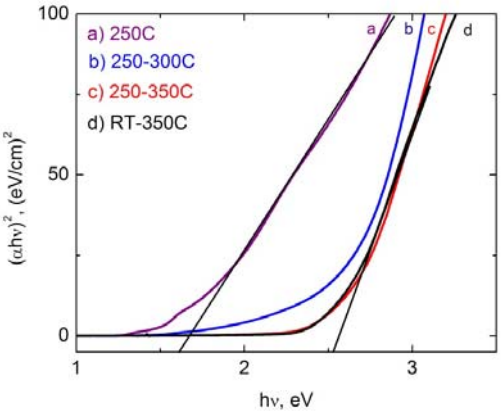

Figure 33. Tauc plots for Sn films sulfurized for 1 hour at (a) 250°C, (b) 250°C and 300°C, (c) 250°C and 350°C, and (d) sulfurizing during the heating from room temperature to 350°C and 1 hour at 350°C.

Carbon Thin Films. The very high chemical affinity of sulfur to react with almost every element of the periodical table and their compounds, especially oxides, causes a technological problem to find a suitable material which would either work as a buffer layer for the conductive back contact or, more desirably, an ohmic contact. Of course, in both cases the material must be resistant to reaction with sulfur. In this study, thin film carbon was tested as the potential candidate for the back contact. So far, two methods were used to deposit carbon thin films, conventional DC magnetron sputtering (MS) and a unique pulsed hollow cathode sputtering (HC) system. In the former case, the graphite target (purity 99.99 %) was sputtered with 200 W of power in a vacuum chamber with the operating pressure level of $1.2x10^{-3}$ Torr. The soda lime glass substrates were kept at 350 °C, 450 °C and 530 °C during deposition. Each of the depositions lasted 1 hour. In addition to the planar target, a hollow cathode utilizing a hollow graphite nozzle was powered via a pulsing unit connected to a DC power supply. The deposition time was 5 hours and the temperature of substrates was maintained at 450 °C. After the deposition, the samples were sulfurized under the same conditions as the α-Fe_2O_3 sol-gel layers.

Figure 34 illustrates the results as determined by Raman spectra which describes the structure of carbon films before and after sulfurization. The two main Raman C - graphite bands termed as D (~ 1340 cm^{-1}) and G (1590 cm^{-1}) bands were identified in the spectra. Whereas in case of magnetron spectra the bands are rather broad, the hollow cathode sputtering gave remarkably sharper and also distinctively separated peaks. Furthermore, the 2D and 2G bands are also present in the spectra. Interesting results were obtained after sulfurization of the samples. A new Raman peak appeared at 1444 cm^{-1} at the spectra of MC – 350 °C and HC. From a patent search [25] it was

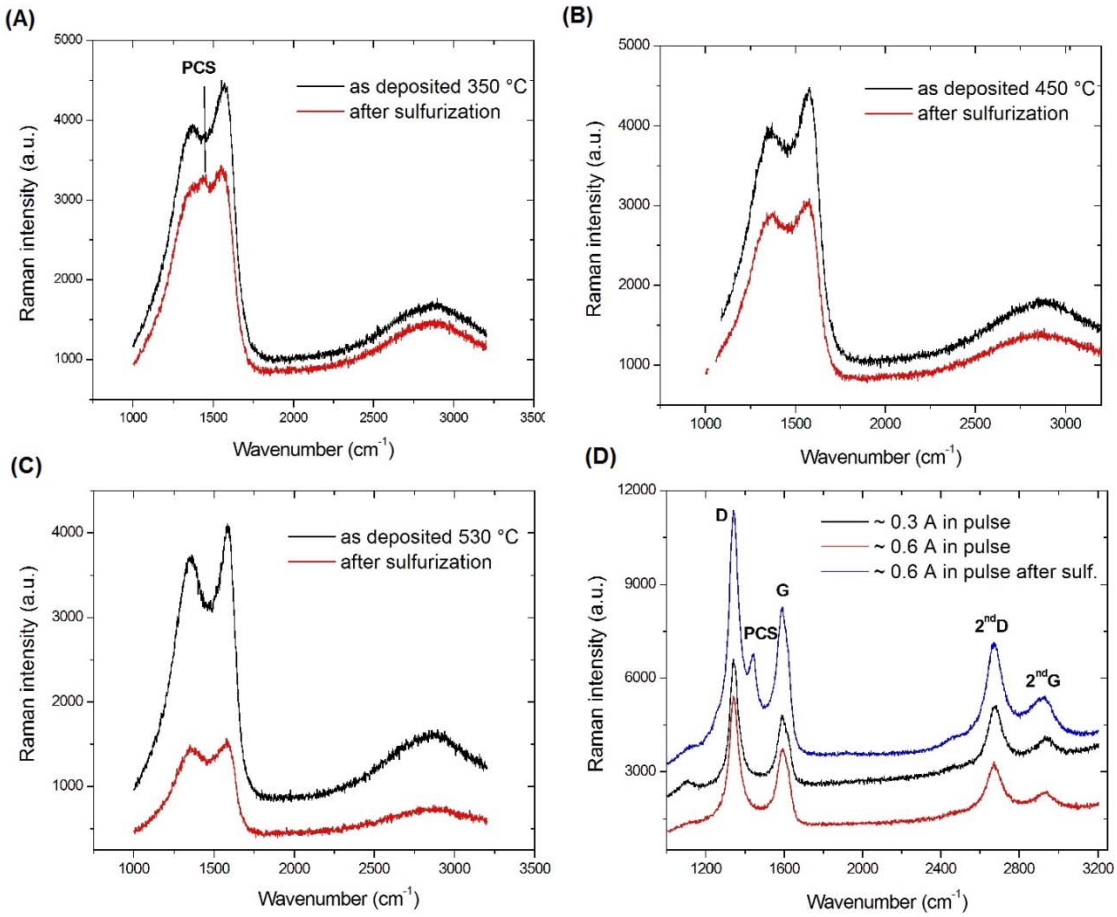

Figure 34. Raman spectra of carbon films: (A) magnetron sputtering at 350 °C of the substrate (MC - 350°C), (B) MC - 450°C, (C) MC - 530°C, (D) hollow cathode sputtering at 450 °C (HC - 450°C).

found that this peak corresponds to polycarbon sulfide. Despite the fact that the carbon layers obviously reacted with the sulfur, it may still be possible to use it as a back contact, as it has been demonstrated that polycarbon sulfide is electrically conductive.. Sulfurized samples were analyzed by Auger electron spectroscopy with the aim to elicit whether the sulfur remains near the surface of the carbon layer or if it penetrates through the film and how much sulfur the samples contained. Figure 35 shows the sulfur content as a function of the number of sputtering cycles in the depth profiling mode of the AES. It was revealed that the amount of sulfur decreased with the temperature of the

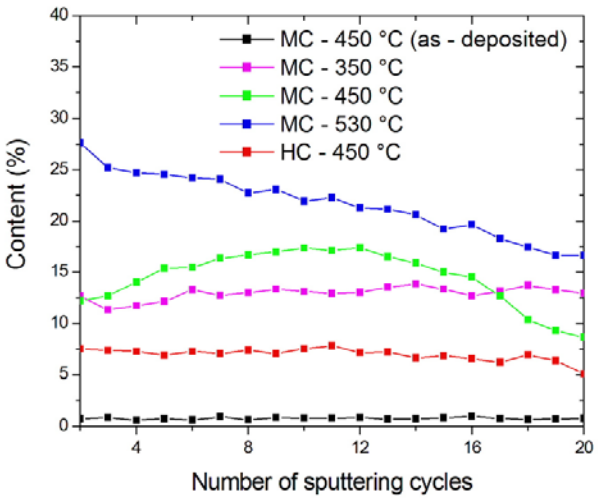

Figure 35. AES depth profile of the carbon layers

samples used during deposition. The lowest sulfur concentration (around 7%) embodied the film prepared by hollow cathode sputtering. This is fortunate in that this deposition technique has been successfully used in the deposition of a large variety of materials in this laboratory [26-31]. The phenomenon is probably connected with the grain sizes, porosity, extent of crystallization, etc. However, these data are still missing. Nevertheless, low concentration of sulfur is very promising and it may be even further reduced by finding the ideal deposition conditions.

References

1. C.L. Exstrom, J. Olejníček, S.A. Darveau, A. Mirasano, D.S. Paprocki, M.L. Schliefert, M.A. Ingersoll, L.E. Slaymaker, R.J. Soukup, N.J. Ianno, C.A. Kamler, *Mater. Res. Soc. Symp. Proc.,* **1165***,* (2009) M05-03.
2. Olejníček, J.; Kamler, C.A.; Darveau, S.A.; Exstrom, C.L.; Slaymaker, L.E.; Vandeventer, A.R.; Ianno, N.J.; Soukup, R.J., *Thin Solid Films* **519**, (2011) 5329-5334.
3. S. Jost, F. Hergert, R. Hock, M. Purwins, R. Enderle, *Phys. Status Solidi A* **203** (2006) 2581.
4. J. López-García, C. Guillén, *Thin Solid Films* **517**, (2009) 2240.
5. Y.B.K. Reddy, V.S. Raja, B. Sreedhar, *J. Phys. D: Appl. Phys.* **39**, (2006) 5124.
6. F. Itoh, O. Saitoh, M. Kita, H. Nagarnori, H. Oike, *Sol. Energ. Mater. Sol. Cells* **50** (1998) 119.
7. L. Roa, J.C. Chervin, A. Chevy, M. Davila, P. Grima, J. Gonzáles, *Phys. Stat. Sol.* **198**, (1996) 99.
8. W. Gebicki, J. Filipowicz, R. Bacewicz, *J. Phys. Condens. Matter* **8**, (1996) 8695.
9. A. Eifler, E.A. Kudritskaya, I.V. Bodnar, V. Riede, *J. Phys. Chem. Solids* **64**, (2003) 1983.
10. Yu. N. Azhnyuk, V.V. Artamonov, I.V. Bodnar, *J. Appl. Spectrosc.* **43**, (1985) 1276.
11. S. Chichibu, A. Kamata, *J. Appl. Phys.* **77**, (1995) 5470.
12. Q. Guo, G.M. Ford, H.W. Hillhouse, and R. Agrawal, *Nano Lett.* **9**, (2009) 3060-3065.
13. Slaymaker, L.E.; Hoffman, N.M.; Ingersoll, M.A.; Jensen, M.R.; Olejníček, J.; Exstrom, C.L.; Darveau, S.A.; Soukup, R.J.; Ianno, N.J.; Amitabha, S.; Kment, Š., *Mater. Res. Soc. Symp. Proc.* **1324**, (2011) DOI: 10.1557/opl.2011.1152.
14. V. Izquierdo-Roca, X. Fontane, L. C. Barrio, J. Alvarez-Garcia, A. Perez-Rodriguez, J. R. Morante, W. Witte, and R. Klenk, *Mater. Res. Soc. Symp. Proc.* **1165**, (2009) M05-16.
15. C. Kamler, R.J. Soukup, N.J. Ianno, J. Huguenin-Love, J. Olejníček, S.A. Darveau, and C.L. Exstrom, *Sol. Energ. Mater. Sol. Cells* **93**, (2009) 45-50.

16. K. Buker, N. Alonso-Vante and H. Tributsch, *J. Appl. Phys.* **72**, (1992) 5721-5728.
17. C. Wadia, A. Paulalvisatos and D.M. Kammen, *Environ Sci. Technol.* **43**, (2009) 2072-2077.
18. S. Fiechter, M. Birkholz. A. Hartmann, P. Dulski, H. Tributsch and R. J. D. Tikkey, *J. Mater. Res.* **7**, (1992) 1829-1838.
19. P. P. Altermat, T Kiesewetter, K. Ellmer and H. Tributsch, *Sol. Energ. Mater. Sol. Cells* **71**, (2002) 181-195.
20. R. Schieck, A. Hartmann, S. Fiechter, R. Konenkamp and H. Wetzel, *J. Mater. Res.* **5,** (1990) 1567.
21. G. Barone, T. G. Hibbert, M. F. Mahon, K. C. Molloy, L. S. Price, I. P. Parkin, A. M. E. Hardy and M. N. Field, *J. Mater. Chem.* **11**, 464 (2001).
22. M. Sugiyama, K. Miyauchi, T. Minemura, *Jap. J.Appl. Phys.* **47,** 4494 (2008).
23. M. Sugiyama, K. Miyauchi, T. Minemura and H. Nakanishi *Jap. J.Appl. Phys.* **47**, 8723 (2008).
24. B. Thangaraju and P. Kaliannan, *J.Phys. D: Appl. Phys.* **33**, 1054 (2000).
25. J. Zhao, S. Ibuki, H. Nishihama, R. Nagai, U.S. Patent no. 6709787 (2004).
26. G. Pribil, Z. Hubička, R. J. Soukup, and N. J. Ianno, *J. Vac. Sci. Technol.* **A19**, 1571-1576 (2001).
27. R. J. Soukup, N. J. Ianno, G. Pribil and Z. Hubička, *Surf. Coatings Technol.* **177-178**, 676-681 (2004).
28. R. J. Soukup, N. J. Ianno, S. A. Darveau, and C. L. Exstrom, *Sol. Energy Mater. Sol. Cells* **87**, 87-98 (2005).
29. J. S. Schrader. J. L. Huguenin-Love, R. J. Soukup, N. J. Ianno, C. L. Exstrom, S. A. Darveau, R. N. Udey, and V. L. Dalal, *Sol. Energy Mater. Sol. Cells* **90**, 2338-2345 (2006).
30. N. J. Ianno, R. J. Soukup, N. Lauer, S. G. Hirsch, C. Hubbard, J. D. Demaree, and M. W. Cole, *Integrated Ferroelectrics* **101**, 63 - 69 (2008).
31. J. Huguenin-Love, N. T. Lauer, R. J. Soukup, N. J. Ianno, Š. Kment, and Z. Hubička, *Mater. Sci. Forum* **245 - 248**, 131 -134 (2010).

Products Developed Under the Award

Journal Article Publications

1. "Thin Films Formed by Selenization of $CuIn_xB_{1-x}$ Precursors in Se Vapor" Kamler, C.; Soukup, R.J.; Ianno, N. J.; Huguenin-Love, J.; Olejníček, J.; Darveau, S.A.; Exstrom, C.L., *Solar Energy Materials and Solar Cells*, **2009**, *93*, 45-50.

2. "Problems with Synthesis of Chalcopyrite $CuIn_{1-x}B_xSe_2$" Olejníček, J.; Darveau, S.A.; Exstrom, C.L.; Soukup, R.J.; Ianno, N.J.; Kamler, C.A.; Huguenin-Love, J.L., *Materials Science Forum*, **2009**, *609*, 33-36.

3. "A Non-vacuum Process for Preparing Nanocrystalline $CuIn_{1-x}Ga_xSe_2$ Materials Involving an Open-air Solvothermal Reaction" Olejníček, J.; Kamler, C.A.; Mirasano, A.*; Martinez-Skinner, A.*; Ingersoll, M.*; Exstrom, C.L.; Darveau, S.A.; Huguenin-Love, J.; Diaz, M.; Ianno, N.J.; Soukup, R.J. *Solar Energy Materials and Solar Cells*, **2010**, *94*, 8-11.

4. "Formation of $CuIn_{1-x}Al_xSe_2$ Thin Films Studied by Raman Scattering," Olejníček, J.; Kamler, C.A.; Darveau, S.A.; Exstrom, C.L.; Slaymaker, L.E.*; Vandeventer, A.R.*; Ianno, N.J.; Soukup, R.J. *Thin Solid Films*, **2011**, *519*, 5329-5334.

5. "$CuIn_{1-x}Al_xS_2$ Thin Films Prepared by Sulfurization of Metallic Precursors," Olejníček, J.; Slaymaker, L.E.*; Darveau, S.A.; Exstrom, C.L.; Kment, Š.; Prabukanthan, P.; Ianno, N.J.; Soukup, R.J. *Journal of Alloys and Compounds*, **2011**, *509*, 10020-10024.

Conference Proceedings

1. "Solvothermal Preparation, Processing, and Characterization of Nanocrystalline $CuIn_{1-x}Al_xSe_2$ Materials" Exstrom, C.L.; Olejníček, J.; Darveau, S.A.; Mirasano, A.*; Paprocki, D.S.*; Schliefert, M.L.*; Ingersoll, M.A.*; Slaymaker, L.E.*; Soukup, R.J.; Ianno, N.J.; Kamler, C.A., *Materials Research Society Symposium Proceedings*, **2009**, *1165*, M05-03.

2. "Self-organized Nanostructures of Vapor-phase Grown $CuGaS_2$ Thin Films", P. Prabukanthan, G. Harichandran, R.J. Soukup, N.J. Ianno, C.L. Exstrom, S.A. Darveau, J. Olejníček, *Proceedings of the 34th IEEE Photovoltaics Specialists Conference*, Philadelphia, PA, June 8-11, 2009.

3. "Room Temperature Non-vacuum Preparation of Nanocrystalline $CuInSe_2$ Employing Aqueous Solvents," Exstrom, C.L.; Darveau, S.A.; Ingersoll, M.A.*; Jensen, M.R.*; Cook, C.*; Slaymaker, L.E.*; Soukup, R.J.; Ianno, N.J., *Proceedings of the 35th IEEE Photovoltaics Specialists Conference*, Honolulu, HI, June 20-25, 2010.

4. "Chemical Bath Deposition (CBD) of Iron Sulfide Thin Films for Photovoltaic Applications, Crystallographic and Optical Properties," Prabukanthan, P.; Soukup, R.J.; Ianno, N.J.; Sarkar, A.; Kamler, C.A.; Exstrom, C.L.; Olejníček, J.; Darveau, S.A., *Proceedings of the 35th IEEE Photovoltaics Specialists Conference*, Honolulu, HI, June 20-25, 2010.

5. "A Novel Method for Synthesis of SnS and SnS_2 Thin Films as Potential Heterjunction Partners for FeS_2 Solar Cells," Sarkar, A.; Soukup, R.J.; Ianno, N.J.; Kamler, C.A.; Exstrom, C.L.; Darveau, S.A.; Olejníček, J., *Proceedings of the 25th European Photovoltaic Solar Energy Conference/5th World Conference on Photovoltaic Energy Conversion*, Valencia, Spain, September 6-10, 2010.

6. "Properties of $CuIn_{1-x}Ga_xSe_2$ Films Prepared by the Rapid Thermal Annealing of Spray-deposited $CuIn_{1-x}Ga_xS_2$ and Se," Slaymaker, L.E.*; Hoffman, N.M.*; Ingersoll, M.A.*; Jensen, M.R.*; Olejníček, J.; Exstrom, C.L.; Darveau, S.A.; Soukup, R.J.; Ianno, N.J.; Sarkar, A.; Kment, Š., *Materials Research Society Symposium Proceedings*, **2011**, *1324*, DOI: 10.1557/opl.2011.1152.

7. "A Novel Sol-Gel Route to Pinhole-Free Iron Sulfide Thin Films," Kment, Š.; Kmentova, H.; Sarkar, A.; Soukup, R.J.; Ianno, N.J.; Krysa, J.; Hubicka, Z.; Olejníček, J.; Exstrom, C.L.; Darveau, S.A., *Proceedings of the 37th IEEE Photovoltaics Specialists Conference*, Seattle, WA, June 19-24, 2011.

Conference Presentations

1. "A Non-vacuum Process for Preparing Nanocrystalline $CuIn_{1-x}Ga_xSe_2$ Materials Involving an Open-air Solvothermal Reaction" Olejnicek, J., Kamler, C.A., Mirasano, A.*, Martinez-Skinner, A.*, Ingersoll, M.*, Exstrom, C.L., Darveau, S.A., Huguenin-Love, J., Diaz, M., Ianno, N.J., Soukup, R.J., *XVII International Materials Research Congress*, Cancun, Mexico, August 2008.

2. "Investigation of Non-vacuum Annealing Process Applied on $Cu(In,Ga)Se_2$, $Cu(In,Al)Se_2$, and $Cu(In,B)Se_2$ Nanocrystals Prepared by Solvothermal Reaction", Olejníček, J.; Darveau, S.A.; Exstrom, C.L.; Mirasano, A.*; Schliefert, M.L.*; Vandeventer, A.R.*; Paprocki, D.S.*; Soukup, R.J.; Ianno, N.J.; Kamler, C.A. *43rd Midwest Regional Meeting of the American Chemical Society*, Kearney, NE, October 8-10, 2008.

3. "Preparation and Characterization of Mixed Indium-Gallium-Selenium Nanocrystalline Materials", Mirasano, A.*; Olejnicek, J.; Exstrom, C.L.; Darveau, S.A.; Soukup, R.J.; Ianno, N.J.; Kamler, C.A. *43rd Midwest Regional Meeting of the American Chemical Society*, Kearney, NE, October 8-10, 2008, and *23rd National Conference on Undergraduate Research*, LaCrosse, WI, April 2009.

4. "Reaction Pathway Investigations of the Solvothermal Preparation of Nanocrystalline $CuInSe_2$ in Chelating Amine Solvents: Effects of Added Salts and Solvent Coordinating Ability", Paprocki, D.S.*; Martinez-Skinner, A.L.*; Ingersoll, M.A.*; Olejnicek, J.; Vandeventer, A.R.*; Mirasano, A.*; Haussler, A.T.*; Exstrom, C.L.; Darveau, S.A.; Huguenin-Love, J.L.; Kamler, C.A.; Diaz, M.; Ianno, N.J.; Soukup, R.J. *43rd Midwest Regional Meeting of the American Chemical Society*, Kearney, NE, October 8-10, 2008.

5. "Use of Surfactant-based Solvents in the Preparation of Nanocrystalline $CuIn_{1-x}M_xSe_2$ (M = Ga, Al, B) Materials", Schliefert, M.L.*; Vandeventer, A.R.*; Mirasano, A.*; Paprocki, D.S.*; Olejnicek, J.; Exstrom, C.L.; Darveau, S.A.; Soukup, R.J.; Ianno, N.J.; Kamler, C.A. *43rd Midwest Regional Meeting of the American Chemical Society*, Kearney, NE, October 8-10, 2008.

6. "Use of Stearate Complexes as Metal Sources in the Preparation of Nanocrystalline $CuIn_{1-x}M_xSe_2$ (M = Ga, B) Materials", Vandeventer, A.R.*; Exstrom, C.L.; Darveau, S.A. *43rd Midwest Regional Meeting of the American Chemical Society*, Kearney, NE, October 8-10, 2008.

7. "Incorporation of Aluminum and Boron into $CuInSe_2$ Chalcopyrite Structures: Preparation and Characterization of the First nanocrystalline $CuIn_{1-x}M_xSe_2$ (M = Al, B) Materials" Exstrom, C.L.; Darveau, S.A.; Olejníček, J.; Schliefert, M.L.*; Paprocki, D.S.*; Vandeventer, A.R.*; Mirasano, A.*; Soukup, R.J.; Ianno, N.J.; Kamler, C.A. *43rd Midwest Regional Meeting of the American Chemical Society*, Kearney, NE, October 10, 2008.

8. "Solvothermal Preparation, Processing, and Characterization of Nanocrystalline $CuIn_{1-x}Al_xSe_2$ Materials" Exstrom, C.L.; Olejnicek, J.; Darveau, S.A.; Mirasano, A.*; Paprocki, D.S.*; Schliefert, M.L.*; Ingersoll, M.A.*; Slaymaker, L.E.*; Soukup, R.J.; Ianno, N.J.; Kamler, C.A. *Materials Research Society Symposium*, San Francisco, CA, April 13-17, 2009.

9. "Self-organized Nanostructures of Vapor-phase Grown $CuGaS_2$ Thin Films", P. Prabukanthan, G. Harichandran, R.J. Soukup, N.J. Ianno, C.L. Exstrom, S.A. Darveau, J. Olejníček, *34th IEEE Photovoltaics Specialists Conference*, Philadelphia, PA, June 8-11, 2009.

10. "Raman Spectroscopy Studies of $CuIn_{1-x}Al_xSe_2$ Thin Film Growth" Olejníček, J.; Exstrom, C.L.; Darveau, S.A.; Vandeventer, A.R.*; Slaymaker, L.E.*; Ianno, N.J.; Soukup, N.J. *238th National Meeting of the American Chemical Society*, Washington, DC, August 16-20, 2009.

11. "Formation of $CuIn_{1-x}Al_xSe_2$ Thin Films Studied by Raman Scattering", J. Olejníček , C.A. Kamler , C.L. Exstrom , S.A. Darveau , N.J. Ianno , R.J. Soukup, *216th Meeting of the Electrochemical Society*, Vienna, Austria, October 4-9, 2009.

12. "Thin Films of $CuIn_xB_{1-x}Se_2$ as Absorbers for CIBS Solar Cells", R. J. Soukup, N. J .Ianno, C. A. Kamler, J. Olejníček, S. A. Darveau, and C. L. Exstrom, *216th Meeting of the Electrochemical Society*, Vienna, Austria, October 4-9, 2009.

13. "Preparation and Studies of Nanocrystalline $CuInSe_2$ Materials Prepared from Aqueous Solution at Room Temperature," Ingersoll, M.A.*; Jensen, M.R.*; Cook, C.*; Slaymaker, L.E.*; Vandeventer, A.R.*; Exstrom, C.L.; Darveau, S.A.; Soukup, R.J.; Ianno, N.J., *44th Midwest Regional Meeting of the American Chemical Society*, Iowa City, IA, October 21-23, 2009.

14. "Effects of Complexing Agents on the Aqueous Solution-based Preparation of Nanocrystalline $CuInSe_2$ and $CuInS_2$ Materials," Jensen, M.R.*; Ingersoll, M.A.*; Cook, C.*; Slaymaker, L.E.*; Vandeventer, A.R.*; Exstrom, C.L.; Darveau, S.A.; Soukup, R.J.; Ianno, N.J., *44th Midwest Regional Meeting of the American Chemical Society*, Iowa City, IA, October 21-23, 2009.

15. "Structural Properties of Poly(vinyl alcohol)-capped Selenium Nanoparticles Prepared from Aqueous Solution," Vandeventer, A.R.*; Slaymaker, L.E.*; Exstrom, C.L.; Darveau, S.A., *44th Midwest Regional Meeting of the American Chemical Society*, Iowa City, IA, October 21-23, 2009.

16. "Effects of Argon Atmosphere on the Selenization of $CuIn_{1-x}Al_x$ and $CuIn_{1-x}B_x$ Thin Films," Slaymaker, L.E.*; Vandeventer, A.R.*; Exstrom, C.L.; Darveau, S.A.; Soukup, R.J.; Ianno, N.J., *44th Midwest Regional Meeting of the American Chemical Society*, Iowa City, IA, October 21-23, 2009.

17. "Use of Sodium Thiosulfate in the Water Solution-based Preparation of Copper Indium Disulfide," Cook, C.*; Ingersoll, M.A.*; Jensen, M.R.*; Slaymaker, L.E.*; Vandeventer, A.R.*; Exstrom, C.L.; Darveau, S.A.; Soukup, R.J.; Ianno, N.J., *44th Midwest Regional Meeting of the American Chemical Society*, Iowa City, IA, October 21-23, 2009.

18. "Low-temperature Aqueous Solution-based Routes for the Preparation of Chalcopyrite Solar Cell Absorber Materials," Exstrom, C.L.; Darveau, S.A.; Ingersoll, M.A.*; Jensen, M.R.*; Cook, C.*; Slaymaker, L.E.*; Vandeventer, A.R.*; Soukup, R.J.; Ianno, N.J. *44th Midwest Regional Meeting of the American Chemical Society*, Iowa City, IA, October 23, 2009.

19. "Room Temperature Non-vacuum Preparation of Nanocrystalline $CuInSe_2$ Employing Aqueous Solvents," Exstrom, C.L.; Darveau, S.A.; Ingersoll, M.A.*; Jensen, M.R.*; Cook, C.*; Slaymaker, L.E.*; Soukup, R.J.; Ianno, N.J., *35th IEEE Photovoltaics Specialists Conference*, Honolulu, HI, June 20-25, 2010.

20. "Chemical Bath Deposition (CBD) of Iron Sulfide Thin Films for Photovoltaic Applications, Crystallographic and Optical Properties," Prabukanthan, P.; Soukup, R.J.; Ianno, N.J.; Sarkar, A.; Kamler, C.A.; Exstrom, C.L.; Olejníček, J.; Darveau, S.A., *35th IEEE Photovoltaics Specialists Conference*, Honolulu, HI, June 20-25, 2010.

21. "A Novel Method for Synthesis of SnS and SnS_2 Thin Films as Potential Heterjunction Partners for FeS_2 Solar Cells," Sarkar, A.; Soukup, R.J.; Ianno, N.J.; Kamler, C.A.; Exstrom, C.L.; Darveau, S.A.; Olejníček, J., *25th European Photovoltaic Solar Energy Conference/5th World Conference on Photovoltaic Energy Conversion*, Valencia, Spain, September 6-10, 2010.

22. "Solvothermal Preparation of Nanocrystalline Pyrite FeS_2 and its Outlook as a Third-generation Solar Cell Absorber Material," Exstrom, C.L.; Darveau, S.A.; Webber, T.E.*; Neville, C.; Slaymaker, L.E.*; Olejníček, J.; Huang, J.; Bi, Y.; Soukup, R.J.; Ianno, N.J.; Amitabha, S., *45th Midwest Regional Meeting of the American Chemical Society*, Wichita, KS, October 28, 2010.

23. "Raman Spectroscopy of $Cu(In,Al)S_2$ Thin Films Prepared by Sulfurization of Metallic Precursors," Olejníček, J.; Darveau, S.A.; Exstrom, C.L.; Slaymaker, L.E.*; Kment, Š.; Soukup, R.J.; Ianno, N.J., *Nebraska Research & Innovation Conference*, Lincoln, NE, October 5, 2010 and *45th Midwest Regional Meeting of the American Chemical Society*, Wichita, KS, October 29, 2010.

24. "$CuIn_xGa_{(1-x)}Se_2$ Films Prepared by Rapid Thermal Annealing of Layered Nanocrystalline $CuIn_xGa_{(1-x)}S_2$ and Se," Slaymaker, L.E.*; Hoffman, N.M.*; Ingersoll, M.A.*; Jensen, M.R.*; Olejníček, J.; Exstrom, C.L.; Darveau, S.A.; Soukup, R.J.; Ianno, N.J.; Amitabha, S., *Nebraska Research & Innovation Conference*, Lincoln, NE, October 5, 2010 and *45th Midwest Regional Meeting of the American Chemical Society*, Wichita, KS, October 29, 2010.

25. "Solvothermal Reaction of Copper and Indium Salts with Sulfur/selenium Mixtures in Oleylamine," Ingersoll, M.A.*; Jensen, M.R.*; Slaymaker, L.E.*; Olejníček, J.; Darveau, S.A.; Exstrom, C.L., *45th Midwest Regional Meeting of the American Chemical Society*, Wichita, KS, October 29, 2010.

26. "Investigation of an Aqueous-based Solution Method for Preparing $CuInSe_2$ using KBH_4 as a Selenium Reducing Agent," Jensen, M.R.*; Hervert, B.A.*; Darveau, S.A.; Exstrom, C.L., *45th Midwest Regional Meeting of the American Chemical Society*, Wichita, KS, October 29, 2010.

27. "Chemical Deposition of Microcrystalline Se Films from Commercial Se Powder in Ethylenediamine Solvent Mixtures," Hoffman, N.M.*; Slaymaker, L.E.*; Olejníček, J.; Exstrom, C.L.; Darveau, S.A.; Soukup, R.J.; Ianno, N.J.; Amitabha, S., *45th Midwest Regional Meeting of the American Chemical Society*, Wichita, KS, October 29, 2010.

28. "Solvothermal Reaction Studies of FeS_2 and SnS_2 Nanoparticle Formation," Webber, T.E.*; Neville, C.; Slaymaker, L.E.*; Olejníček, J.; Darveau, S.A.; Exstrom, C.L.; Soukup, R.J.; Ianno, N.J.; Amitabha, S., *45th Midwest Regional Meeting of the American Chemical Society*, Wichita, KS, October 29, 2010.

29. "Properties of $CuIn_{1-x}Ga_xSe_2$ Films Prepared by the Rapid Thermal Annealing of Spray-deposited $CuIn_{1-x}Ga_xS_2$ and Se," Slaymaker, L.E.*; Neville, C.; Hoffman, N.M.*; Ingersoll, M.A.*; Jensen, M.R.*; Olejníček, J.; Exstrom, C.L.; Darveau, S.A.; Soukup, R.J.; Ianno, N.J.; Amitabha, S.; Kment, Š., *Materials Research Society Symposium*, San Francisco, CA, April 25-29, 2011.

30. "Raman spectroscopy of $Cu(In,Al)S_2$ thin films prepared by sulfurization of metallic precursors," Olejníček, J.; Darveau, S.A.; Exstrom, C.L.; Slaymaker, L.E.*; Kment, Š.; Soukup, R.J.; Ianno, N.J., *Materials Research Society Symposium*, San Francisco, CA, April 25-29, 2011.

31. "A Novel Sol-Gel Route to Pinhole-Free Iron Sulfide Thin Films," Kment, Š.; Kmentova, H.; Sarkar, A.; Soukup, R.J.; Ianno, N.J.; Krysa, J.; Hubicka, Z.; Olejníček, J.; Exstrom, C.L.; Darveau, S.A., *37th IEEE Photovoltaics Specialists Conference*, Seattle, WA, June 19-24, 2011.

32. "Solvothermal Preparation of Nanocrystalline SnS_2 via Hot-Injection and Thermal Decomposition Methods," Exstrom, C.L.; Darveau, S.A.; Webber, T.E.*; Jensen, M.R.*; Ingersoll, M.A.*; Neville, C.; Soukup, R.J.; Ianno, N.J.; Amitabha, S., *242nd National Meeting of the American Chemical Society*, Denver, CO, August 28-29, 2011.